Advances in Environmental Technology 2 (2017) 67-75

Advances in Environmental Technology

journal homepage: http://aet.irost.ir

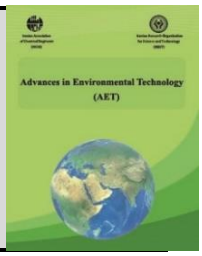

Nanostructured Fe_2O_3/Al_2O_3 adsorbent for removal of As (V) from water

Faranak Akhlaghian[1*], Bubak Souri[2], Zahra Mohamadi[1]

[1]*Department of Chemical Engineering, Faculty of Engineering, University of Kurdistan, Sanandaj, Iran*

[2]*Department of Environmental Science, Faculty of Natural Resources, University of Kurdistan, Sanandaj, Iran*

ARTICLE INFO

Article history:
Received 7 February 2017
Received in revised form
24 August 2017
Accepted 25 August 2017

Keywords:
Adsorption
Arsenate
Fe_2O_3/Al_2O_3
Immobilization
Water treatment

ABSTRACT

The presence of arsenate in drinking water causes adverse health effects including skin lesions, diabetes, cancer, damage to the nervous system, and cardiovascular diseases. Therefore, the removal of As (V) from water is necessary. In this work, nanostructured adsorbent Fe_2O_3/Al_2O_3 was synthesized via the sol-gel method and applied to remove arsenate from polluted waters. First, the Fe_2O_3 load of the adsorbent was optimized. The Fe_2O_3/Al_2O_3 adsorbent was characterized by means of XRF, XRD, ASAP, and SEM techniques. The effects of the operating conditions of the batch process of As (V) adsorption such as pH, adsorbent dose, contact time, and initial concentration of As (V) solution were studied, and optimized. The thermodynamic study of the process showed that arsenate adsorption was endothermic. The kinetic model corresponded to the pseudo-second-order model. The Langmuir adsorption isotherm was better fitted to the experimental data. The Fe_2O_3/Al_2O_3 adsorbent was immobilized on leca granules and applied for As (V) adsorption. The results showed that the immobilization of Fe_2O_3/Al_2O_3 on leca particles improved the As (V) removal efficiency.

1. Introduction

Arsenic enters our water sources through the leaching of soils and rocks, mining, smelting, disposal of industrial wastewater, and pesticides [1,2]. High concentrations of arsenic in drinking water is a serious problem in many countries such as India, Bangladesh, Taiwan, Mongolia, China, and Chile [3,4]. Exposure to arsenic causes diseases such as skin, lung, and bladder cancers, gastrointestinal disorders, and cardiovascular and cerebrovascular diseases [1,4,5]. The World Health Organization (WHO) recommends limiting arsenic concentration in drinking water to 10 µg/L [4]. There are several methods for removing arsenic from water such as adsorption, coagulation, precipitation, membrane, and ion exchange. Among these methods, adsorption is the most promising because of its low cost, simple operation, and non-harmful by products [6]. Many researches have focused on developing adsorbents to efficiency remove arsenic from water. Jeong et al. [7] compared iron and aluminum oxides as inexpensive adsorbents for As (V) removal and found that Fe_2O_3 was a better adsorbent than Al_2O_3. Savina et al. [8] studied the removal of As (V) by applying iron nanoparticles embedded with macroporous polymer composites. Chen et al. [9] found that the high efficiency of As (V) adsorption on Ce-Fe bimetal oxide was related to its adsorbent mesoporous structure and abundant surface hydroxyl groups. Kong et al. [10] studied the role of an adsorbent of magnetic nanoscale Fe-Mn binary oxides loaded zeolites in the removal of arsenic from water. In most of the works, the adsorbents were in nano size powder forms which are difficult and expensive to separate from treated water [11]. The immobilization of adsorbent on substrate improves adsorption efficiency makes adsorbent separation from water easier in batch processes, and results in a lower pressure drop in column processes [11]. Therefore, in this work, the nanostructured Fe_2O_3/Al_2O_3 was synthesized via the sol-gel method and applied for the adsorption of As (V) from water. Also, Fe_2O_3/Al_2O_3 immobilized on leca granules was investigated for the adsorption of As (V) from water.

*Corresponding author. Tel: +98 87 33664600
E-mail address: akhlaghianfk@gmail.com
DOI: 10.22104/AET.2017.2003.1099

2. Materials and methods

Aluminum isopropoxide (98%), iron (III) nitrate (98%), ethanol (98%), nitric acid (65%), sodium arsenate (98%), and polyethylene glycol with a molecular weight of 2000 g/gmol were purchased from Merck Company. The leca granules were purchased from Leca Company (Iran).

2.1. Synthesis of Fe_2O_3/Al_2O_3

In order to prepare the Fe_2O_3/Al_2O_3, double distilled water was added to aluminum isopropoxide, and hydrolyzed. The molar ratio of aluminum isopropoxide to water was 1:100. The mixture was stirred at a constant rate and heated to 85°C. Then, nitric acid was added to pepitize alumina sols. The molar ratio of water to acid was 1:0.07. Then, iron (III) nitrate was added. The mixture was stirred at 85°C under reflux for 24 h. The obtained gel was dried in an oven at 100°C for 12 h [12,13]. The dried gel was calcined at 400°C for 2 h. The synthesized particles were crushed, and sieved to the particles size of 60-90 µm.

2.2. Immobilization on leca particles

Leca granules with diameters of 4 to 10 mm were used as substrate. First, leca granules were cleaned for coating; so they were placed in a beaker containing nitric acid (10 wt.%) and exposed to ultrasonic waves for 30 min. Afterwards, the leca particles were rinsed with double distilled water and dried at 100°C in an oven for 24 h. The coating slurry was prepared by mixing distilled water (70 mL), polyethylene glycol (15 gr), nitric acid (1 g), and synthesized adsorbent (15 g). For 24 h, the mixture was stirred at a constant rate. The leca granules were coated by the dip coating method. They were immersed in the coating slurry, and then pulled out at a constant speed. The coated particles were dried at 100°C for 12 h [14]. Ultrasonic testing was used to examine the adhesion of the adsorbent to the substrate. A certain amount of coated granules was immersed in a beaker containing water, then it was exposed to ultrasonic waves for 30 min. The weight loss below 10% showed that the adsorbent particles were well adhered to the leca substrate [15]. The adsorbent was immobilized on the leca particles in this way.

2.3. Characterization

An X-ray fluorescence (XRF) spectrometer of Philips PW 2404 was used to determine the elemental composition of the adsorbent. The X-ray powder diffraction (XRD) analysis was performed using an X'Pert MPD Philips spectrometer with Co-k_α irradiation. The data were collected at 0.2°/s of scanning speed in the range of 10-80°. The specific surface area and pore volume were measured by nitrogen adsorption-desorption using an ASAP 2010 Micrometrics. The sample morphology was observed by a MIRA3 field emission scanning electron microscope from TESCAN.

2.4. Adsorption experiments of Fe_2O_3/Al_2O_3

The adsorbent dose of 1 g/L was added to 100 mL of arsenate synthetic wastewater with the concentration of 50 mg/L. The mixture was stirred at room temperature (25°C) for 12 h. Then, the mixture was centrifuged, and the arsenate concentration of the solution was determined by a Phoenix 986 atomic absorption spectrometer. The efficiency of the arsenate removal was calculated through Equation (1):

$$\text{Removal efficiency } \% = 100 \times \left(\frac{C_0 - C_f}{C_f}\right) \quad (1)$$

where C_0, and C_f are the initial, and final concentration of arsenate in the water solution; respectively.

2.5. Adsorption studies

Adsorption experiments were performed to understand the behavior, nature, kinetics, and thermodynamics of the process. The effect of temperature on the adsorption of As (V) on Fe_2O_3/Al_2O_3 was examined. In Equation (2) [16,17]

$$K = \frac{mq_e}{C_e} \quad (2)$$

K is the equilibrium constant; q_e (mg/g) is equilibrium adsorption capacity; C_e (mg/L) is the equilibrium concentration of As (V) in the solution; and m is the adsorbent mass.

In Equation (3) [16,17]:

$$\text{Log } K = \frac{\Delta S}{2.3R} - \frac{\Delta H}{2.3RT} \quad (3)$$

R is the universal gas constant, and 8.314 J/mol.K; T (K) is temperature. K (equilibrium constant) was determined at different temperature using Equation (2). ΔH (enthalpy) and ΔS (entropy) can be determined from the slope (-ΔH/2.3R) and intercept (ΔS/R) of the linear plot of Log (K) versus 1/T.

From Equation (4) [16,17]:

$$\Delta G = \Delta H - T\Delta S \quad (4)$$

Gibbs free energies were calculated at different temperatures [16,17].

The pseudo-first-order and pseudo-second-order models were employed to study the kinetics of the adsorption process. The pseudo-first-order (Equation (5)) and pseudo-second-order (Equation (6)) models are shown below [6,18]:

$$\text{Log}(Q_e - Q_t) = \text{Log}Q_e - \frac{k_1}{2.303}t \quad (5)$$

$$\frac{t}{Q_t} = \frac{1}{k_2 Q_e^2} + \frac{t}{Q_e} \quad (6)$$

where Q_e (mg/g) is equilibrium adsorption capacity; Q_t (mg/g) is adsorption capacity at any time t (min); k_1 and k_2 are rate constants of the pseudo-first-order and pseudo-

second-order models; respectively. The Langmuir and Freundlich isotherm models were used for fitting of the experimental data. The Freundlich isotherm is expressed as follows [18]:

$$\mathrm{Log}q = \frac{1}{n}\mathrm{Log}C_e + \mathrm{Log}K_F \quad (7)$$

where n is a constant related to the adsorption energy; K_F K_F $(mg^{1-1/n}L^{1/n}/g)$ is a constant related to adsorption capacity.

The Langmuir isotherm model is shown below [18]:

$$\frac{1}{q} = \frac{1}{q_m b C_e} + \frac{1}{q_m} \quad (8)$$

where q_m is the maximum adsorption capacity; b (L/g) is a constant related to the adsorption energy; q (mg/g) is the As (V) concentration in the solid adsorbent; and C_e is the As (V) concentration in the solution (mg/L).

3. Results and discussion

3.1. Characterization

XRF spectrometry was used to determine the adsorbent composition. The composition of the optimized adsorbent was determined as 37.6%Fe_2O_3/62.4%Al_2O_3. The X-ray diffraction patterns of the Al_2O_3 and 37.6%Fe_2O_3/62.4%Al_2O_3 synthesized adsorbents are shown in Figure 1. The Al_2O_3 XRD pattern show the formation of amorphous alumina [19]. In the XRD pattern of Fe_2O_3/Al_2O_3, the peaks observed at 28.22°, 38.77°, 41.75°, 47.945°, 58.2°, 64.105°, 74.345°, and 76.005° were related to the formation of Fe_2O_3 with rhombohedral lattice (JCPDS File No. 13-0534) [20,21].

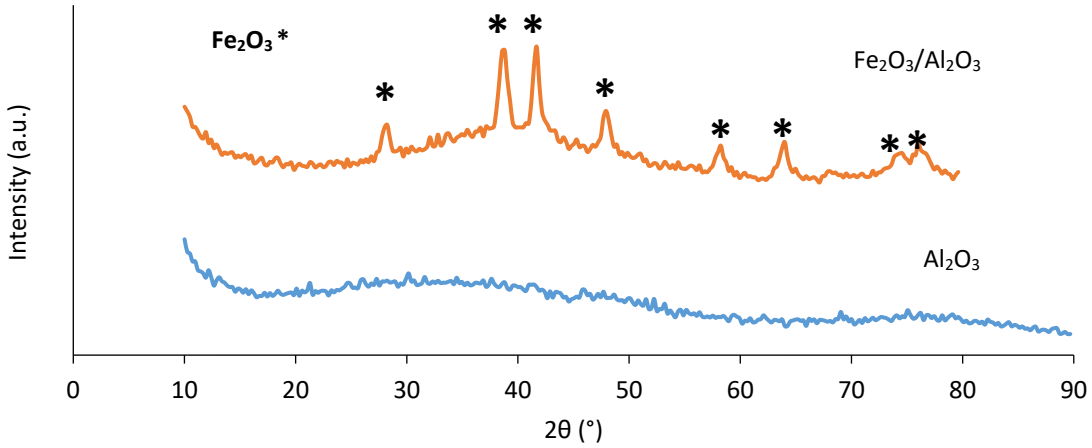

Fig.1. XRD pattern of Al_2O_3 and Fe_2O_3/Al_2O_3 adsorbents

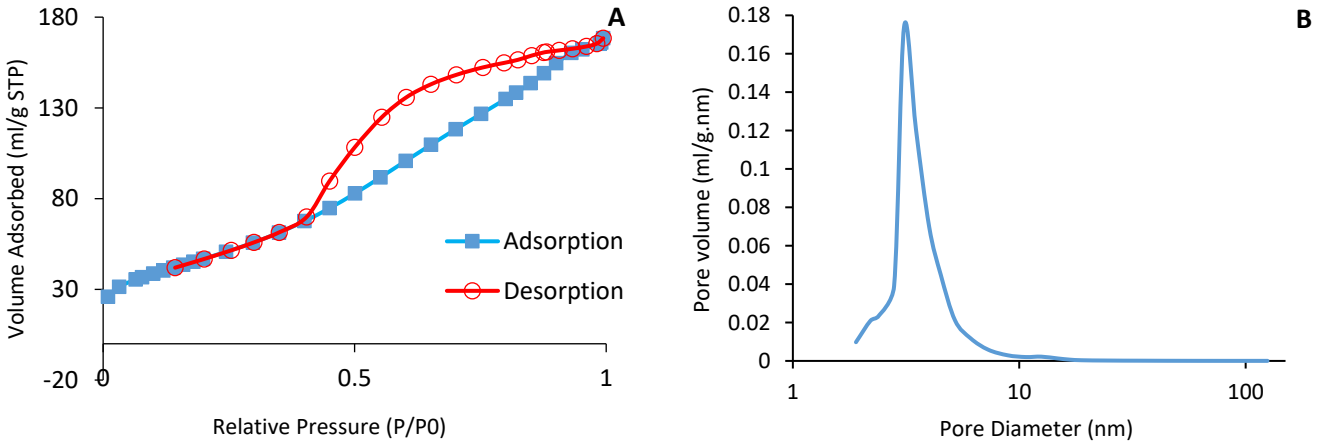

Fig. 2. (A) Liquid nitrogen adsorption/desorption isotherm of 37.6%Fe_2O_3/62.4%Al_2O_3; (B) Pore size distribution of 37.6%Fe_2O_3/62.4%Al_2O_3 based on BJH desorption model

Figure 2(A) displays nitrogen adsorption/desorption isotherms of the 37.6%Fe_2O_3/62.4%Al_2O_3 adsorbent which is a mesopore of type IV according to the IUPAC classification. The hysteresis loop is type H2, showing pores with large bodies and small mouths. Figure 2 (B) shows the pore size distribution in the range of 2-100 nm which is

unimodal with a peak at 3.1 nm [22]. The specific surface area, total pore volume, and average pore diameter were determined as 269.151 cm^2/g, 0.260451 cm^3/g, and 3.9565 nm, respectively, based on the BJH desorption model. The SEM images of the 37.6%Fe_2O_3/62.4%Al_2O_3 adsorbent are shown in Figure 3 and dispersed nano size Fe_2O_3 particles are observed. The size of the Fe_2O_3 particles are less than 100 nm.

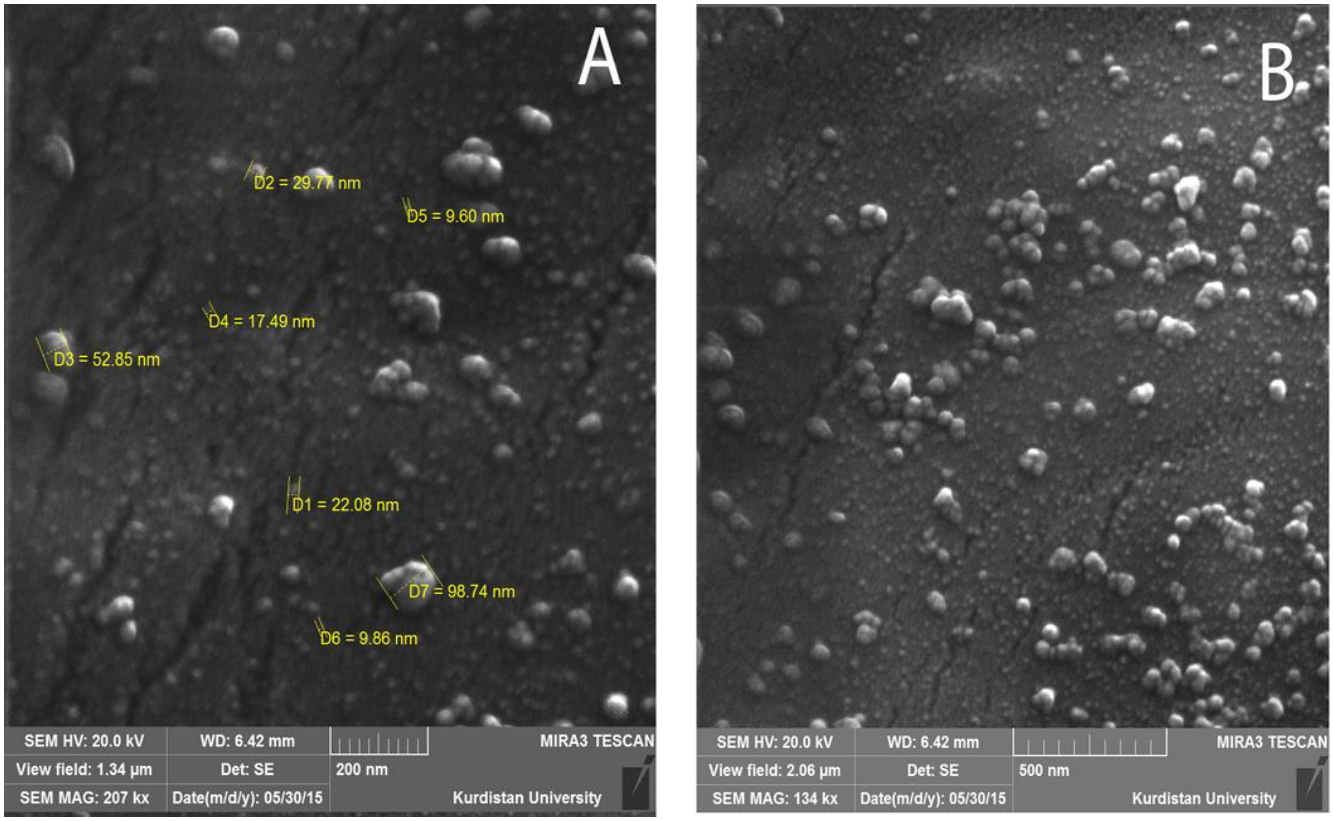

Fig. 3. SEM images of 37.6%Fe_2O_3/62.4%Al_2O_3 adsorbent

3.2. *Optimization of the adsorbent*

The Fe_2O_3/Al_2O_3 adsorbents with different amounts of iron were synthesized and applied for the adsorption of As (V) from synthetic wastewater. Figure 4 shows the removal of As (V) with different amounts of iron in Fe_2O_3/Al_2O_3 adsorbents. Arsenic adsorption increased with the increase of Fe_2O_3 content from 0 to 37.6% by weight. An increase of Fe_2O_3 content increased the active sites favored by As (V) adsorption. However, the increase of Fe_2O_3 over 37.6% decreased As (V) adsorption. This could be related to the agglomeration of active sites [6].

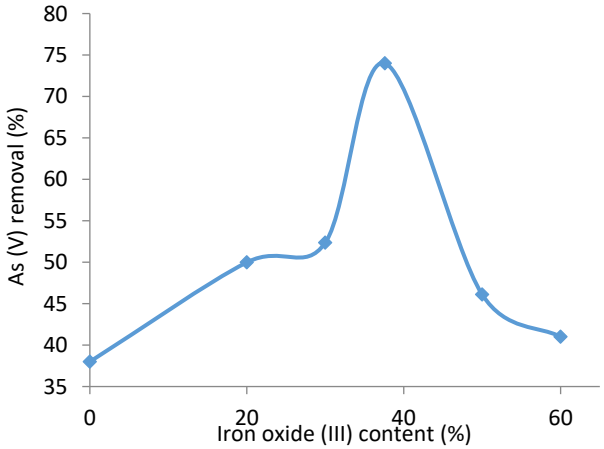

Fig. 4. The effect of Fe_2O_3 content on As (V) removal; operating conditions: As (V) initial concentration 50 mg/L, pH 6, adsorbent dose 1 g/L, contact time 12 h

3.3. Optimization of operating conditions

3.3.1. Effect of pH

The effect of pH on As (V) adsorption is shown in Figure 5 (A). In the pH range of 4 to 7, adsorption was nearly constant. In the pH of 7, adsorption was 72.61%. This amount dropped to 41.16% in the pH of 10. In the pH range of 2 to 10, As (V) occurs in the forms of $H_2AsO_4^-$ and $HAsO_4^{2-}$ [23]. The pH of zero point charge was 7. In pH<pHzpc, the adsorbent is positively charged because of the high concentration of protons in the solution and protonation. The attractive columbic force between the positively charged surface and negatively charged As (V) species led to adsorption. In pH>pHzpc, the adsorption decreased due to repulsive columbic force between the negatively charged surface and As (V) ions as well as the competition for adsorption between hydroxyl groups and As (V) species [23-25].

3.3.2. Effect of adsorbent dose

The adsorption increased with increasing of the adsorbent dose from 0.5 to 1 g/L (Figure 5 (B)). Increasing the available active site and specific surface area improved the adsorption. The adsorption remained nearly constant due to the agglomeration of adsorbent particles in the adsorbent dose more than 1 g/L [26].

3.3.3. Effect of contact time

In the first 120 min of the adsorption reaction, the rate was high, and then it became nearly constant (Figure 5(C)). In the first 120 min of adsorption, 64% of the As (V) was removed while in 720 min of adsorption, 74% of As (V) was removed. This high rate of adsorption in the first minutes is related to the large number of available surface sites. After sometime, the adsorption rate declined and finally reached equilibrium. The reason for the slow adsorption rate was the small number of active sites. At this stage, the adsorption reaction proceeded through the internal active sites of the adsorbent [27].

3.3.4. Effect of arsenate initial concentration

Figure 5 (D) shows that increasing arsenate initial concentration decreased adsorption. The saturation of the available sites with increasing of the arsenate concentration decreased the adsorption [27].

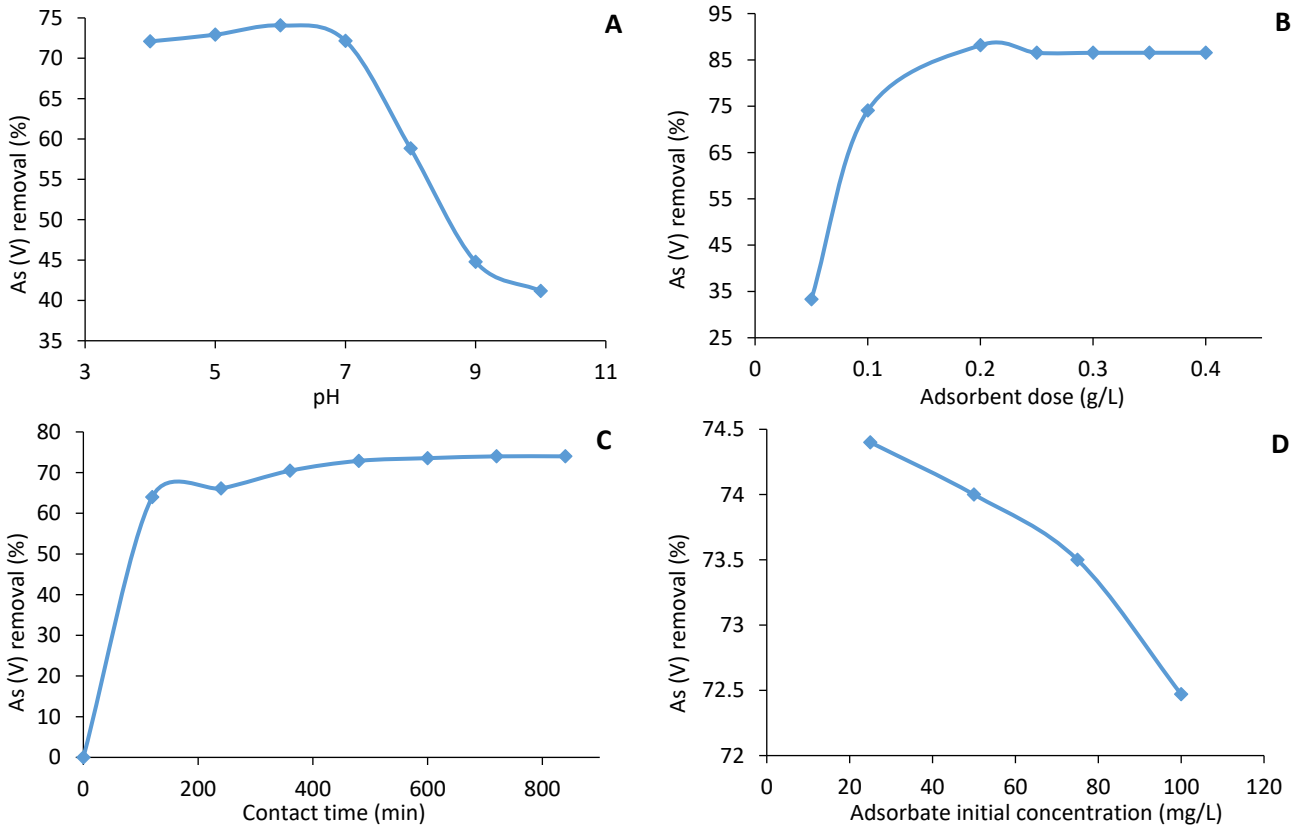

Fig. 5. Effects of operating conditions on As (V) removal (A) pH, (B) adsorbent dose, (C) contact time, (D) As (V) initial concentration. instead of; in the above figure, the operating conditions of As (V) initial concentration 50 mg/L, pH 6, adsorbent dose 1 g/L, and contact time 12 h were constant unless their effect was investigated

3.4. Thermodynamic, kinetics, and isotherms of adsorption

The results of the raising temperature showed slightly increased As (V) adsorption on 37.6%Fe_2O_3/62.4%Al_2O_3. Equations (2) and (3) were used at different temperatures. The ΔH was calculated (+65.96 kJ/mol) showing it was an endothermic process. The ΔS was determined to be 228.87 J/mol presenting increased randomness at the interface of the solid solution for As (V) adsorption. Gibbs free energies were calculated at different temperatures by Equation (4) which is shown in Table 1.

Table 1. Thermodynamic data for As (V) adsorption by 37.4% Fe_2O_3/62.6%Al_2O_3; operating condition: As (V) initial concentration 50 mg/L, pH 6, adsorbent dose 1g/L, contact time 12 h

T (K)	K	ΔG	ΔS (J/mol)	ΔH
298	2.97	-2.24	228.87	65.96
303	3.11	-3.39		
313	5.13	-5.13		
318	10.47	-10.47		

The values of Gibbs free energies were negative indicating the spontaneous process of As (V) adsorption [16,17]. The mechanism of As (V) adsorption on the 37.6%Fe_2O_3/62.4%Al_2O_3 adsorbent was studied using Equations (5) and (6). The determination factor R^2 of the pseudo-second order model is larger than the pseudo-first-order model (Table 2), so it can be concluded that the kinetics obeyed the pseudo-second-order model and chemisorption is the controlling step of the adsorption [6,18]. The results of curve fitting are displayed in Figure (6). Table 3 shows the determination factor R^2 for fitting the experimental data of As (V) adsorption on alumina to Freundlich and Langmuir isotherms. The larger determination factor R^2 shows that adsorption followed the Langmuir isotherm model. Similarly, Table 3 shows R^2s for the 37.6%Fe_2O_3/62.4%Al_2O_3 adsorbent. The Langmuir isotherm model was better fitted to the experimental data due to the larger R^2 compared with the Freundlich model. For alumina maximum adsorption capacity, q_m was 40.65 mg/g and b was 0.0275 L/mg (Table 3). For the adsorbent 37.6%Fe_2O_3/62.4%Al_2O_3, q_m was 74.6 mg/g and b was 0.0392 L/mg. The larger adsorption capacity indicates that 37.6%Fe_2O_3/62.4%Al_2O_3 is a more efficient adsorbent for the removal of As (V) from water compared with alumina.

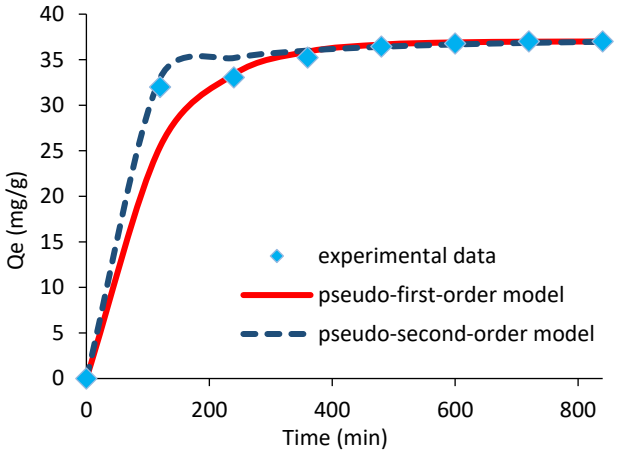

Fig. 6. Kinetics of As (V) adsorption on 37.6%Fe_2O_3/62.4%Al_2O_3 adsorbent

Table 2. Kinetic parameters for As (V) adsorption by 37.6%Fe_2O_3/62.4%Al_2O_3 adsorbent

Pseudo-first-order model				
Q_e (mg/g)	k_1 (min^{-1})	Q_1 (mg/g)	R^2	Variance
37.01	0.0097	36.017	0.9468	10.87
Pseudo-second-order model				
Q_e (mg/g)	k_2 (g/mg.min)	Q_2 (mg/g)	R^2	Variance
37.01	0.0015	37.7	0.9989	1.53

Table 3. Isotherm model parameter for As (V) by Al_2O_3, 37.6%/Fe_2O_3/62.4%Al_2O_3; operating conditions: pH 6, adsorbent dose 1g/L, contact time 12 h

Model	Parameter	Al_2O_3	37.6%/Fe_2O_3/62.4%Al_2O_3
Freundlich equation	K_F ($mg^{1-1/n}L^{1/n}/g$)	2.97	2.87
	n	1.93	0.992
	R^2	0.9679	0.997
	Variance	0.093	0.0743
Langmuir equation	q_m (mg/g)	40.65	74.6
	b (L/mg)	0.0275	0.0392
	R^2	0.9769	0.999
	Variance	0.0067	0.0052

3.5. Adsorption of immobilized adsorbent

The leca was coated by the 37.6%Fe_2O_3/62.4%Al_2O_3 adsorbent and applied for As (V) adsorption. The coating layer load on leca particles was 4% by weight (Figure 7). The calculation of the immobilized adsorbent dose according to its load is given in the caption of Figure 7. The adsorption of As (V) improved using immobilized adsorbent on leca

granules due to increasing available surface area. In the batch process, the immobilized adsorbent on the leca granules separated more easily from water. In the column process, the leca granules increased the porosity of the bed and decreased the pressure drop.

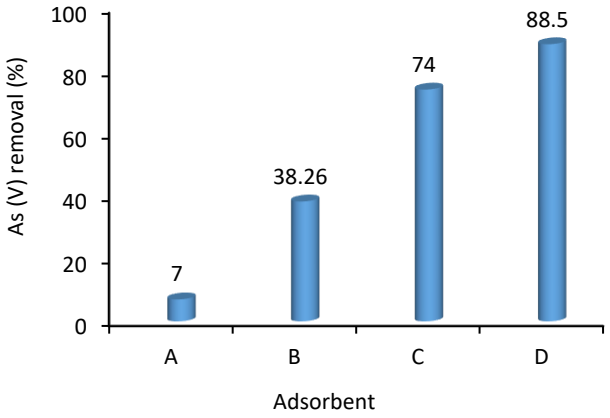

Fig. 7. As (V) adsorption on different adsorbents (A) leca, (B) alumina, (C) 37.6%Fe_2O_3/Al_2O_3, (D) coated leca; operating conditions: As (V) initial condition 50 mg/L, pH 6, contact time 12 h, adsorbent dose (A) 50 g/L, (B) 1 g/L, (C) 1g/L, (D) 50 g/L (50 g of coated leca $\times$ (4 g coating layer)/ (100 g of coated leca) $\times$ $1/2 = 1$ g of $37.6\%Fe_2O_3/62.4\%Al_2O_3$), the ratio of 37.6%$Fe_2O_3$/62.4%$Al_2O_3$ to polyethylene glycol+ 37.6%Fe_2O_3/62.4%Al_2O_3 in coating slurry was 1/2, so in our calculation we multiplied the result by 1/2.

Table 4 shows the results of fitting Langmuir and Freundlich isotherms to the experimental data for the immobilization of 37.6%Fe_2O_3/62.4%Al_2O_3 on leca particles (coated leca). The larger R^2 reveals that Langmuir isotherm model fitted the experimental data better. The results of this work are compared with other literature works in Table 5. It is clear that the best adsorption capacity belonged to 37.6%Fe_2O_3/62.4%Al_2O_3 on leca. The adsorption capacity of 37.6%Fe_2O_3/62.4%Al_2O_3 was also good. These results suggest that the Fe-Al binary metal adsorbent prepared with the proposed method as well as coating it on a substrate like leca can be very efficient for the removal of As (V) from water.

Table 4. Isotherm model parameter for As (V) adsorption by coated leca; operating conditions: pH 6, adsorbent dose 1g/L, contact time 12 h

Model	Parameter	coated leca
Freundlich equation	K_F ($mg^{1-1/n}L^{1/n}/g$)	2.094
	n	0.678
	R^2	0.776
	Variance	0.429
Langmuir equation	q_m (mg/g)	125
	b (L/mg)	0.1
	R^2	0.999
	Variance	0.0313

Table 5. Comparisons of As (V) adsorption capacities of different adsorbents

No.	Adsorbent	Adsorption capacity (mg g^{-1})	Reference
1	Al_2O_3	0.17	[7]
2	Fe_2O_3	0.66	[7]
3	Iron oxide particles-embedded macroporous polymers	91.74	[9]
4	Fe-Al double hydrous oxide	24.1	[11]
5	Cryogel embedded with Fe-Al double hydrous oxide	24.6	[11]
6	Ni-Fe binary oxide	90.1	[29]
7	Iron-ziconia coated sand	45.05	[28]
8	Al_2O_3	40.65	present work
10	37.6%Fe_2O_3/62.4%Al_2O_3	74.6	present work
11	37.6%Fe_2O_3/62.4%Al_2O_3 coated on leca	125	Present work

Conclusions

The Fe_2O_3/Al_2O_3 adsorbent was synthesized using aluminum isopropoxide and iron (III) nitrate as precursors via the sol-gel method. The synthesized adsorbent was used for the adsorption of As (V) from water. The load of iron oxide of the adsorbent was optimized and the XRF results determined the composition of the adsorbent 37.6%Fe_2O_3/62.4%Al_2O_3. The XRD results showed the formation of hematite Fe_2O_3 and amorphous Al_2O_3. The SEM images depicted nano size iron oxide particles. The kinetics studies revealed that As (V) adsorption of 37.6%Fe_2O_3/62.4%Al_2O_3 obeyed the pseudo-second-order model. The Langmuir isotherm model fitted the experimental data better than Freundlich model. The adsorption capacity of pure Al_2O_3 and 37.6%Fe_2O_3/62.4%Al_2O_3 were determined to be 40.65 and 74.6 mg/g, respectively. The adsorption capacity of 37.6%Fe_2O_3/62.4%Al_2O_3 coated on leca was determined to be 125 mg/g which revealed its higher efficiency in respect to uncoated adsorbents. A comparison of the adsorption capacity of the nanostructured 37.6%Fe_2O_3/62.4%Al_2O_3 adsorbent with those available in the literature revealed that this adsorbent is promising.

Acknowledgments

The financial support of the University of Kurdistan is gratefully acknowledged.

References

[1] Shevade, S., Ford, R. G. (2004). Use of synthetic zeolites for arsenate removal from pollutant water. *Water research*, *38*(14), 3197-3204.

[2] Reza, R., Singh, G. (2010). Heavy metal contamination and its indexing approach for river water. *International journal of environmental science and technology*, *7*(4), 785-792.

[3] Kundu, S., Kavalakatt, S. S., Pal, A., Ghosh, S. K., Mandal, M., Pal, T. (2004). Removal of arsenic using hardened paste of Portland cement: batch adsorption and column study. *Water research*, *38*(17), 3780-3790.

[4] Sigdel, A., Park, J., Kwak, H., Park, P. K. (2016). Arsenic removal from aqueous solutions by adsorption onto hydrous iron oxide-impregnated alginate beads. *Journal of industrial and engineering chemistry*, *35*, 277-286.

[5] Sigdel, A., Park, J., Kwak, H., Park, P. K. (2016). Arsenic removal from aqueous solutions by adsorption onto hydrous iron oxide-impregnated alginate beads. *Journal of industrial and engineering chemistry*, *35*, 277-286.

[6] Han, C., Zhang, L., Chen, H., Shan, X., Li, X., Zhu, W., Luo, Y. (2016). Removal As (V) by sulfated mesoporous Fe–Al bimetallic adsorbent: Adsorption performance and uptake mechanism. *Journal of environmental chemical engineering*, *4*(1), 711-718.

[7] Jeong, Y., Fan, M., Singh, S., Chuang, C. L., Saha, B., Van Leeuwen, J. H. (2007). Evaluation of iron oxide and aluminum oxide as potential arsenic (V) adsorbents. *Chemical engineering and processing: Process intensification*, *46*(10), 1030-1039.

[8] Savina, I. N., English, C. J., Whitby, R. L., Zheng, Y., Leistner, A., Mikhalovsky, S. V., Cundy, A. B. (2011). High efficiency removal of dissolved As (III) using iron nanoparticle-embedded macroporous polymer composites. *Journal of hazardous materials*, *192*(3), 1002-1008.

[9] Chen, B., Zhu, Z., Guo, Y., Qiu, Y., Zhao, J. (2013). Facile synthesis of mesoporous Ce–Fe bimetal oxide and its enhanced adsorption of arsenate from aqueous solutions. *Journal of colloid and interface science*, *398*, 142-151.

[10] Kong, S., Wang, Y., Hu, Q., Olusegun, A. K. (2014). Magnetic nanoscale Fe–Mn binary oxides loaded zeolite for arsenic removal from synthetic groundwater. *Colloids and surfaces A: Physicochemical and engineering aspects*, *457*, 220-227.

[11] Kumar, P. S., Önnby, L., Kirsebom, H. (2013). Arsenite adsorption on cryogels embedded with iron-aluminium double hydrous oxides: Possible polishing step for smelting wastewater. *Journal of hazardous materials*, *250*, 469-476.

[12] Chen, H., Bednarova, L., Besser, R. S., Lee, W. Y. (2005). Surface-selective infiltration of thin-film catalyst into microchannel reactors. *Applied catalysis A: General*, *286*(2), 186-195.

[13] Germani, G., Alphonse, P., Courty, M., Schuurman, Y., Mirodatos, C. (2005). Platinum/ceria/alumina catalysts on microstructures for carbon monoxide conversion. *Catalysis today*, *110*(1), 114-120.

[14] Germani, G., Stefanescu, A., Schuurman, Y., Van Veen, A. C. (2007). Preparation and characterization of porous alumina-based catalyst coatings in microchannels. *Chemical engineering science*, *62*(18), 5084-5091.

[15] Stefanescu, A., Van Veen, A. C., Mirodatos, C., Beziat, J. C., Duval-Brunel, E. (2007). Wall coating optimization for microchannel reactors. *Catalysis today*, *125*(1), 16-23.

[16] Goswami, A., Raul, P. K., Purkait, M. K. (2012). Arsenic adsorption using copper (II) oxide nanoparticles. *Chemical engineering research and design*, *90*(9), 1387-1396.

[17] Xiong, C., Li, Y., Wang, G., Fang, L., Zhou, S., Yao, C., Zhu, Y. (2015). Selective removal of Hg (II) with polyacrylonitrile-2-amino-1, 3, 4-thiadiazole chelating resin: batch and column study. *Chemical engineering journal*, *259*, 257-265.

[18] Wu, K., Liu, T., Xue, W., Wang, X. (2012). Arsenic (III) oxidation/adsorption behaviors on a new bimetal adsorbent of Mn-oxide-doped Al oxide. *Chemical engineering journal*, *192*, 343-349.

[19] Amini, G., Najafpour, G. D., Rabiee, S. M., Ghoreyshi, A. A. (2013). Synthesis and Characterization of Amorphous Nano-Alumina Powders with High Surface Area for Biodiesel Production. *Chemical engineering and technology*, *36*(10), 1708-1712.

[20] Biabani-Ravandi, A., Rezaei, M., Fattah, Z. (2013). Catalytic performance of Ag/Fe_2O_3 for the low temperature oxidation of carbon monoxide. *Chemical engineering journal*, *219*, 124-130.

[21] Golsefidi, M.A., Abbasi, F., Abrodi, M., Abbasi, Z., Yazarlou, F. (2016). Synthesis characterization and photocatalytic activity of Fe_2O_3-TiO_2 nanoparticles and nanocomposite. *Journal of nanostructures, 6* (1), 61-66.

[22] Leofanti, G., Padovan, M., Tozzola, G., Venturelli, B. (1998). Surface area and pore texture of catalysts. *Catalysis today*, *41*(1), 207-219.

[23] Sahiner, N., Ozay, O., Aktas, N., Blake, D. A., John, V. T. (2011). Arsenic (V) removal with modifiable bulk and nano p(4-vinylpyridine)-based hydrogels: The effect of hydrogel sizes and quarternization agents. *Desalination*, *279*(1), 344-352.

[24] Zheng, Y. M., Zou, S. W., Nanayakkara, K. N., Matsuura, T., Chen, J. P. (2011). Adsorptive removal of arsenic from aqueous solution by a PVDF/zirconia blend flat sheet membrane. *Journal of membrane science*, *374*(1), 1-11.

[25] Kumar, A. S. K., Jiang, S. J. (2016). Chitosan-functionalized graphene oxide: A novel adsorbent an efficient adsorption of arsenic from aqueous solution. *Journal of environmental chemical engineering*, *4*(2), 1698-1713.

[26] Lisha, K. P., Maliyekkal, S. M., Pradeep, T. (2010). Manganese dioxide nanowhiskers: a potential adsorbent for the removal of Hg (II) from water. *Chemical engineering journal*, *160*(2), 432-439.

[27] Nath, B. K., Chaliha, C., Kalita, E., Kalita, M. C. (2016). Synthesis and characterization of ZnO: CeO 2: nanocellulose: PANI bionanocomposite. A bimodal agent for arsenic adsorption and antibacterial action. *Carbohydrate polymers*, *148*, 397-405.